Desalination and Water Treatment
www.deswater.com
doi: 10.5004/dwt.2023.29561

295 (2023) 95–104
May

Heterogeneous catalytic ozonation by amorphous copper silicate for degradation of *p*-chloronitrobenzene in water

Congmin Wang, Yue Liu*, Quan Zhao, Rong Guo, Yanyan Dou, Caixia Zhu

School of Energy and Environment Engineering, Zhongyuan University of Technology, Zhengzhou 451191, China, Tel.: +86-0371-62503050; email: yue5757@sina.com (Y. Liu)

Received 15 November 2022; Accepted 7 April 2023

ABSTRACT

An amorphous copper silicate catalyst was prepared using $Cu(NO_3)_2$ and $Na_2SiO_3{\cdot}9H_2O$ as precursors. Characterization of amorphous copper silicate was accomplished by several techniques, including X-ray diffraction, X-ray photoelectron spectroscopy analysis, scanning electron microscopy, transmission electron microscopy, thermogravimetry-differential thermal curves, Fourier-transform infrared spectroscopy, and nitrogen adsorption–desorption. The results of characterization showed that Cu–Si binary oxide and CuO were formed on the surface of amorphous copper silicate and contained abundant functional groups. The dosages of the catalyst, ozone, and humic acid affected the removal efficiency of *p*-chloronitrobenzene (*p*-CNB). A hydroxyl radical (•OH) scavenger experiment, electron spin resonance (ESR) analysis, and pH experiment demonstrated that •OH was the predominant reactive specie for *p*-CNB degradation. Catalytic reusability studies demonstrated that amorphous copper silicate maintained its catalytic activity and stability for five consecutive cycles.

Keywords: Catalytic ozonation; Amorphous copper silicate; Hydroxyl radicals; *p*-Chloronitrobenzene

1. Introduction

Ozone is a powerful oxidant (E_0 = 2.07 V) that is widely used in drinking water and wastewater reclamation treatments [1]. However, several drawbacks—including longer required reaction time, high energy consumption, low mineralization rate, low oxidation potential of ozone molecules, and non-effective degradation of carboxylic acid groups—have limited the practical applications of the ozonation process [2]. To overcome these restrictions and improve the ability of ozone to degrade organic compounds, ozone has recently been integrated with some techniques like UV/O_3, US/O_3, H_2O_2/O_3, and catalytic ozonation. By decomposing ozone using a catalyst, catalytic ozonation produces oxidative radicals, such as hydroxyl radicals, •OH, which react very quickly with many organic species. These radicals enable organic pollution to be decomposed and mineralized [3].

There are two types of catalytic ozonation: homogeneous and heterogeneous. In homogeneous catalytic ozonation, several transition metal ions have been used, including Mn^{3+} [4], Fe^{3+} [5], Co^{2+} [6], and Cu^{2+} [7]. However, metal ion catalysts that are soluble in water are difficult to separate after a reaction, thus having the possibility to act as pollutants. In heterogeneous catalytic ozonation, ozone is catalyzed by a solid catalyst. Heterogeneous catalytic ozonation has the potential for real-world applications in water and wastewater treatment because, unlike homogeneous ozonation, it is highly efficient, does not require additional sources of energy, such as thermal or light energy, and does not generate secondary pollution [8].

Over the past few decades, many solid catalysts have been used for heterogeneous catalytic ozonation, including metal oxides (e.g., MnO_2 [9], TiO_2, Al_2O_3, CeO_2) [10,11], transition metals (Cu, Co, Ni) on supports (TiO_2, Al_2O_3, and CeO_2) [12,13], zeolites modified with metals [14–16], and

* Corresponding author.

activated carbon [17]. The copper oxide was found to be a promising catalyst because it is chemically stable, low cost, and non-toxic, and it can reduce ozone consumption and increase reaction rates [18–20]. However, power copper oxide catalysts are generally not used in water treatment due to the difficulty in separating them from treated water.

As functional materials, metal silicates have recently been fabricated due to their unique properties of uniform mesoporous channel structure, good chemical stability, high surfaces area, low density, good adsorption capacity, low cost, and high number of hydroxyl groups. There are several applications for this catalyst, such as the decomposition of nitrophenols [21], methylene blue dye [22], nitrobenzene [23], and diclofenac [24]. $Cu(NO_3)_2$ is a strong acid-weak base salt that forms $[Cu(H_2O)_6]^{2+}$ when dissolved in water. Sodium silicate is a strong base-weak acid salt that forms $Si(OH)_4$ when dissolved in water. When a solution of $Cu(NO_3)_2$ is mixed with a solution of Na_2SiO_3, silico-metal surface complexes are likely to form between Si and Cu. The complexation of Cu and Si may increase the physical strength of the synthesized product. In this study, a new type of amorphous copper silicate catalyst embedded with copper oxides and silicon oxides was synthesized.

The halogenated nitro-aromatic compound *p*-chloronitrobenzene (*p*-CNB) is widely used in the production of pesticides, gasoline additives, antioxidants, herbicides, dyes, photographic films, and other industrial chemicals. Although *p*-CNB has been detected in many lakes and rivers [25], the traditional water treatment process has low *p*-CNB degradation efficiency. In comparison to the reaction rate constants for *p*-CNB with $^{\bullet}OH$ and with O_3, *p*-CNB scarcely reacts with molecule ozone [26].

The purpose of the present study was to synthesize and identify the characteristics of amorphous copper silicate as an ozonation catalyst, and to investigate its catalytic performance in the ozonation of *p*-CNB in an aqueous solution.

2. Experimental set-up

2.1. Chemicals and reagents

Milli-Q ultra-pure water (specific resistance P18 MX cm) was used to prepare all solutions. By dissolving 100 mg *p*-CNB into 1,000 mL ultra-pure water, a 100 mg/L *p*-CNB (99.5% purity, Chem Service, USA) stock solution was prepared. 5,5-dimethyl-1-pyrroline N-oxide (DMPO, >97%) were purchased from USA Chem service. Methanol was purchased from Sigma-Aldrich (USA) and was high-performance liquid chromatography (HPLC) grade. The chemicals used were sodium hydroxide, copper nitrate, hydrochloric acid, sodium thiosulfate, *t*-butanol, indigo, phosphoric acid, and sodium silicate, all of which were analytical grade.

2.2. Synthesis of catalyst

$Cu(NO_3)_2$ and $Na_2SiO_3{\cdot}9H_2O$ were used as precursors to synthesize copper silicate catalysts. At room temperature, 150 mL of $Cu(NO_3)_2$ solution was slowly added to 200 mL of Na_2SiO_3 solution at 1 mL/min. Meanwhile, the magnetic stirrer was turned on and rotated at 200 rpm. By adding NaOH solution (0.1 M) to the suspension, the pH was adjusted to 12 before being aged for 24 h at 60°C in a muffle furnace. The precipitate was collected and then washed several times in ultra-pure water until the pH and conductivity remained constant. After drying at 90°C, the precipitate was ground. It was found that the as-synthesized copper silicate was reproducible. To further study the physical and chemical properties of copper silicate (90°C), the other copper silicate catalysts (800°C) were prepared by calcined copper silicate (90°C) samples at 800°C for 4 h.

2.3. Experimental procedure

The catalytic ozonation experiments were carried out in batch mode at a temperature of 20°C under thermostatic control. A flat-bottomed flask with a volume of 1.2 L served as the reactor. For each experiment, 1 L of ultrapure water was added to the reactor. Ozone gas was produced from pure oxygen (Harbin Gas Co. Ltd., 99.999%, China) through a CF-G-3-010 g ozone generator (Qingdao Guolin, China). Ozone was bubbled into the reactor for the desired period using a silicate dispenser to obtain the desired concentration. The initial aqueous ozone concentration was controlled by changing the electrical current of the ozone generator. After that, the catalyst was added to the stock ozone solution along with the *p*-CNB stock solution. In parallel, the reactor was sealed and the magnetic stirrer was switched on to continuously mix the suspension. In the experiments, 25 mL suspensions collected from the reactor were quenched immediately by adding $Na_2S_2O_3$ solution (0.1 mol/L) after a designated period. The quenched suspension was passed through a 0.45 μm filter prior to the analysis of residual *p*-CNB concentration. Identical experimental conditions were used for both the adsorption on copper silicate and ozonation experiments. NaOH solution (0.1 mol/L) and H_3PO_3 solution (0.1 mol/L) were used to adjust the pH of the solution.

2.4. Analytical method

An Agilent 1200 HPLC System (Agilent, USA) was used to determine the concentration of *p*-CNB using a reversed-phase 4.6 mm × 250 mm C18 waters column at room temperature. At a flow rate of 1.0 mL/min, methanol, and water (8:2 v/v) were pumped together for elution. An SPD-10A UV-Vis Detector was used at a wavelength of 265 nm. To determine mineralization, TOC-VCPH analysis was performed. X-ray diffraction (XRD) analysis was carried out on a Bruker D8 Advance Diffractometer with Cu Kα radiation (λ = 1.5418 Å) to evaluate the crystalline structures of the catalyst. An Axis Ultra Instrument from Kratos was used to measure the chemical composition of the products using monochromatic Al Kα radiation (225 W, 15 mA, 15 kV). An FEI Tecnai G2 F30 (Japan) was used to examine the morphologies and sizes of samples. A Surface Area and Porosity Analyzer (Micromeritics ASAP 2020, USA) was used to measure the catalyst's surface area. Fourier-transform infrared spectroscopy (FTIR) was used to analyze the surface properties of the catalyst. An STA-449C thermal analyzer was used to record thermogravimetry-differential thermal curves (TG-DTG). A saturated deprotonation method described by Laiti et al. [27] was used to measure the density of surface hydroxyl groups. An inductively coupled plasma

atomic emission spectrometer (ICP-AES, Optima 5300DV, Perkin Elmer, USA) was used to identify metals leaching from the catalyst into the solution. The indigo method [28] was used to determine the concentration of ozone in an aqueous solution.

3. Results and discussion

3.1. Catalyst characterization

The copper silicate XRD pattern in Fig. 1a shows no sharp, intense peak, but instead a rather broad, low-intensity, vaguely recognizable peak. This indicated that the as-synthesized copper silicate had an amorphous structure caused by the inhibitory effects of the highly dispersed silica sol formed from the hydrolysis of sodium silicate. As the calcination temperature rose from 90°C to 800°C, amorphous copper silicate completely crystallized. According to JCPDS Card No. 29-85, the first highest peak was characteristic of SiO_2. In addition, there were several small and relatively strong peaks, which appeared in close agreement with CuO (Card No. 89-5896). This result indicated that copper silicate (800°C) was mainly composed of CuO and SiO_2.

X-ray photoelectron spectroscopy (XPS) analysis was carried out on copper silicate to understand its surface chemistry. Fig. 1b shows that the wide Cu 2p3/2 obviously shifted to a low position after deconvolution and could be fitted satisfactorily to two principal peaks; CuO was responsible for the peak at 941.5 eV [29], and Cu–O–Si binary oxidation for the peak at 937.4 eV. Additionally, a higher binding energy 103.1 eV (Fig. 1c) was observed for the Si 2p peak compared with pure SiO_2 crystal (100.2 eV). Cu–O–Si binary oxidation could explain the shifts of the Cu 2p3/2 and Si 2p peaks. The O 1s XPS spectra in Fig. 1d show asymmetric peaks, indicating different degrees of oxygen contribution. They corresponded to Cu–O (531.1 eV), Cu–O–Si binary oxides (529.8 eV), Si–O–Si (533.4eV), and adsorbed water (532.2 eV), respectively [29].

As shown in Fig. 2, there were abundant ball-like particles in the typical scanning electron microscopy (SEM) image. These ball-like particles were the CuO crystallites present inside the amorphous silica sol.

The transmission electron microscopy (TEM) image of the as-obtained amorphous copper silicate is shown in Fig. 3. There were numerous particles embedded in the amorphous silica matrix. Fig. 3a shows the SAED pattern, indicating that some crystallites were present in the particles. Fig. 3b shows the high-resolution transmission electron microscopy (HR-TEM) pattern of a single particle and its corresponding fast Fourier-transform (FFT) pattern. The interlayer distance was calculated to be about 0.186 nm, which corresponded to the 111 planes of CuO [30]. The HR-TEM image and FFT pattern confirmed that there were some CuO crystallites embedded within the amorphous silica matrix.

The physicochemical sorption properties and pore parameters of copper silicate were determined by nitrogen adsorption–desorption measurement. Fig. 4 shows that

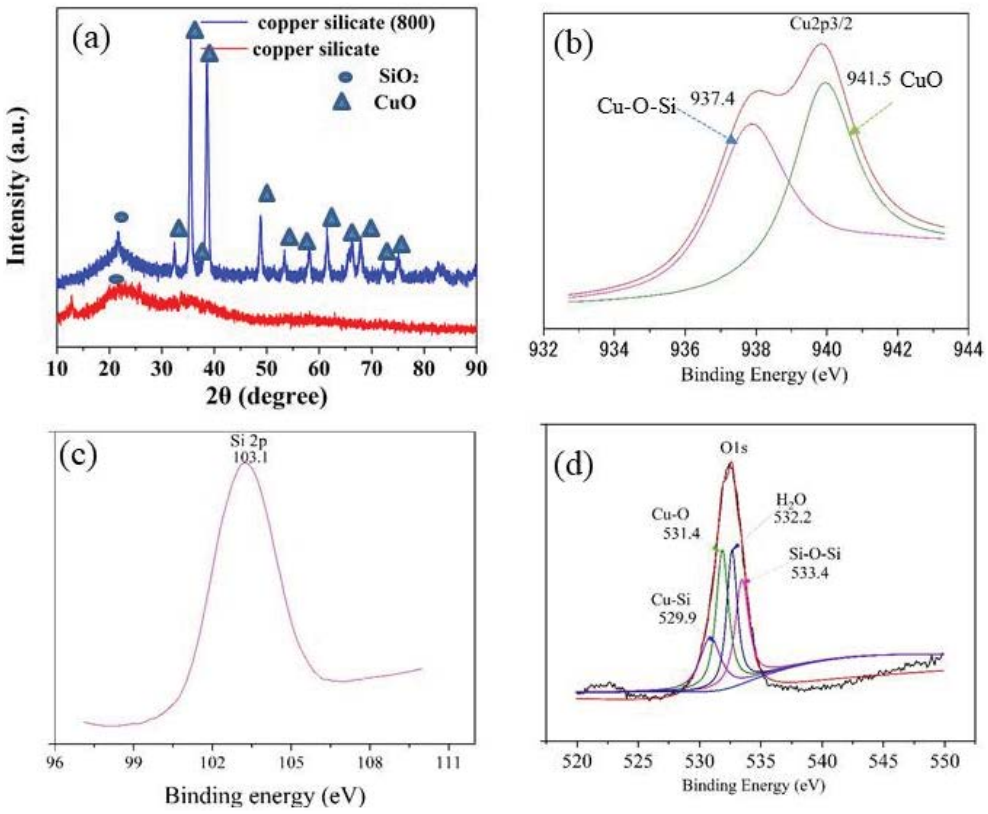

Fig. 1. (a) X-ray diffraction analysis of copper silicate calcined at different temperature, (b) Cu 2p3/2 spectrum, (c) Si 2p spectrum and (d) O 1s spectrum.

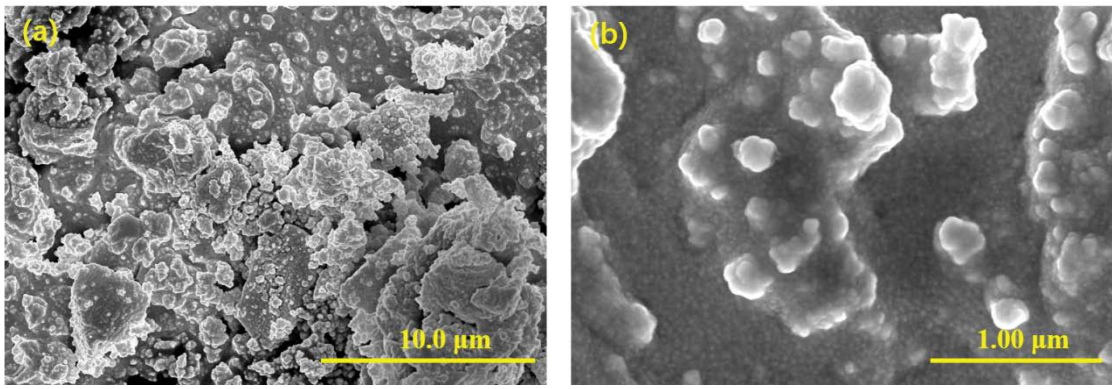

Fig. 2. (a) Scanning electron microscopy photographs of the amorphous copper silicate sample (a) ×2,000 and (b) ×10,000.

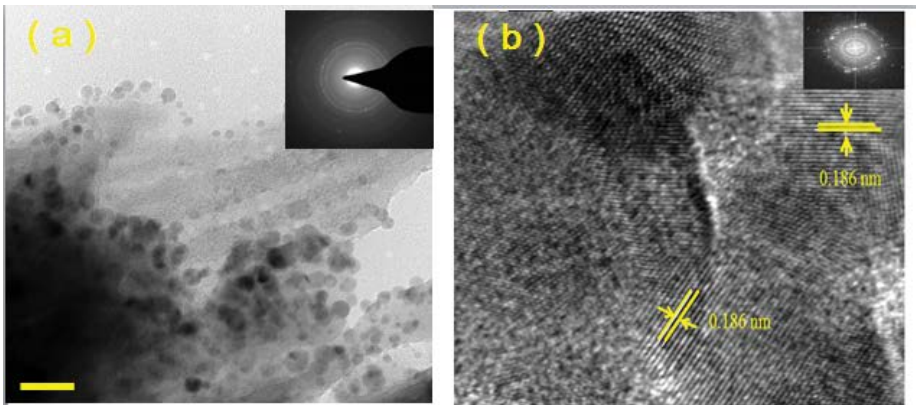

Fig. 3. (a) Transmission electron microscopy image of the copper silicate sample. (b) High-resolution transmission electron microscopy image of a single CuO particle.

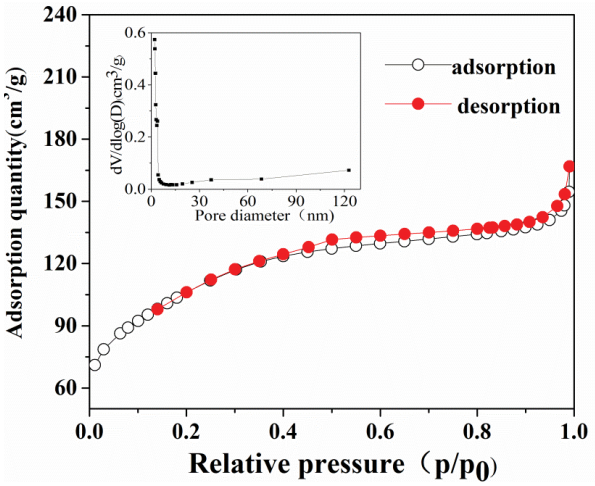

Fig. 4. Nitrogen adsorption–desorption isotherm of copper silicate. The inset shows its BJH pore-size distribution curve.

copper silicate exited typical type-IV-like isotherms [31]. There was a distinct H_2 hysteretic loop at 0.4 relative pressures, indicating a mesoporous structure. The inset in Fig. 4 is the pore-size distribution plot, which was created using the Barrett–Joyner–Halenda (BJH) method from the desorption branch of the isotherm. Mesopore size distributions ranged from 2.1 to 130 nm. Copper silicate had an average pore diameter of 4.45 nm. A wide distribution indicated that copper silicate had a significant ozone and organic matter adsorption capacity. Copper silicate had a Brunauer–Emmett–Teller (BET) surface area of 247.1 m^2/g and a pore volume of 0.41 cm^3/g.

To confirm the bonding states of the elements, FTIR characterization was conducted on copper silicate, and the results are shown in Fig. 5a. The band at 3,462 cm^{-1} corresponded to the stretching of hydroxyl groups of absorbed water, and the band at 1,637 cm^{-1} corresponded to the bending vibration of absorbed water [32]. The band at 1,375 cm^{-1} was associated with hydroxyl deformation vibrations of hydrated copper oxide. Spectra at 670 cm^{-1} were attributed to binary oxide Cu–O–Si [33]. The absorbance at 472 cm^{-1} originated from the Cu–O bond. Saturated deprotonation experiments showed that the density of surface hydroxyl groups on amorphous copper silicate was 1.73×10^{-2} mol/g. Moreover, according to the TG-DTG results (Fig. 5b), significant weight loss and an endothermic peak were observed near 100°C and 260°C, indicating the evaporation of adsorbed water and dehydroxylation, respectively [34]. This phenomenon reveals that amorphous

copper silicate had abundant surface hydroxyl groups. These surface hydroxyl groups are extremely useful for catalytic ozonation and catalytic ozone destruction [35].

3.2. Catalytic activity

Through ozonation of *p*-CNB, the catalytic activities of the as-synthesized amorphous copper silicate and CuO were evaluated. Fig. 6a shows that in the ozonation system, only approximately 55% of *p*-CNB was removed in 20 min. This indicated that ozonation alone could not completely oxidize *p*-CNB. In the adsorption experiment, during the same period, *p*-CNB removal was about 3% in the presence of amorphous copper silicate and 5.1% in the presence of CuO. This indicated that neither amorphous copper silicate nor CuO could adsorb *p*-CNB very well. Moreover, the degradation rates of *p*-CNB in the systems of O_3/amorphous copper silicate and O_3/CuO were 98.3% and 82.5%, respectively. Compared with the cumulative effect of ozone alone and the adsorption of amorphous copper silicate, an increment of approximately 40% of *p*-CNB degradation was observed during the amorphous copper silicate catalytic ozonation process. The experimental results suggested that the presence of the amorphous copper silicate catalyst had a synergistic effect with ozone for the degradation of *p*-CNB.

To further investigate the catalytic activity of the amorphous copper silicate and CuO in mineralizing *p*-CNB, the total organic carbon (TOC) was measured during the reactions in this study, and the results are illustrated in Fig. 6b. TOC removal by ozonation alone was 27.3%, whereas TOC removal by amorphous copper silicate catalytic ozonation reached 57.3% within 20 min, so amorphous copper silicate was superior to O_3/CuO for TOC removal. A comparison of the amorphous copper silicate and CuO regarding the removal of TOC indicated that amorphous copper silicate was more active than CuO in the catalytic ozonation of *p*-CNB.

In order to confirm the performance of copper silicate/O_3 system for removing *p*-CNB, those reported various catalysts under similar reaction conditions were compared and summarized in Table 1. The degradation efficiency of *p*-CNB are higher than those in previous reported literature, suggesting that the copper silicate/O_3 system exhibits efficient catalytic performance towards *p*-CNB.

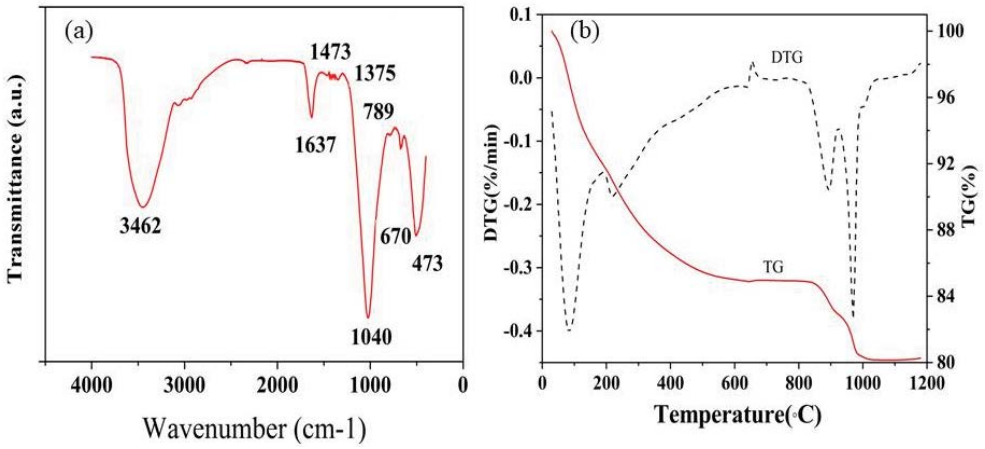

Fig. 5. (a) Fourier-transform infrared spectrum of the copper catalyst. (b) Thermogravimetry-differential thermal curves spectrum of the copper catalyst.

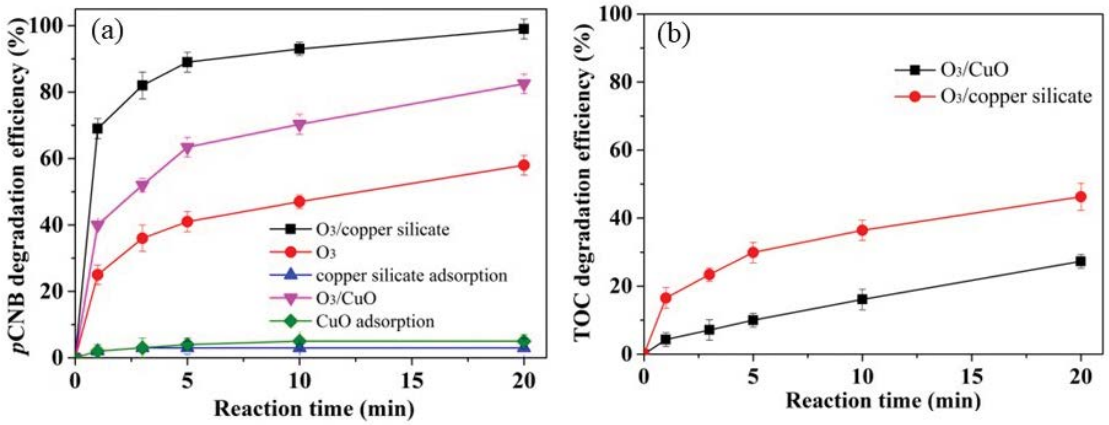

Fig. 6. (a) Degradation of *p*-CNB vs. reaction time. (b) Degradation of TOC vs. reaction time. Experiment conditions: $[p\text{-CNB}]_0$ = 100 μg/L, $[O_3]_0$ = 0.8 mg/L, [catalysts] = 100 mg/L, solution pH = 8.0, T = 20°C.

Table 1
Comparisons of degradation of *p*-CNB by various catalysts with ozone

Catalysts (mg/L)	*p*-CNB (mg/L)	Ozone (mg/L)	Removal efficiency	Reaction duration (min)	References
α-Fe(Fe^{2+})OOH 50	0.05	0.6	57.2%	10	[16]
Pumice 1,000	0.1	0.6	86.5%	20	[15]
Fe/pumice 500	0.1	0.9	90.8%	15	[20]
Amorphous zinc silicate 100	0.1	0.6	98.9%	15	[36]
Zinc-copper silicate polymer 300	0.1	0.6	99.3%	15	[25]
S-MnO_2 membrane 300	0.1	0.5	61.5%	20	[37]
Copper silicate 100	0.1	0.8	98.3%	20	This study

From the above analysis, it was deduced that (1) the presence of amorphous copper silicate has a significant impact on the ozone for the degradation of *p*-CNB and (2) compared with CuO, amorphous copper silicate can stimulate ozone to decompose to produce more active species. According to the results of XRD, XPS, SEM, and TEM analysis, copper silicate was mainly composed of Cu–O–Si binary oxides and CuO. These results indicated that the Cu–O–Si binary oxide played an excellent synergistic role in improving the catalytic activity.

3.3. Analyzing the effects of parameters on the catalytic ozonation of p-CNB with copper silicate

3.3.1. Effect of ozone dosage

In this study, the effect of ozone dosage on catalytic ozonation degradation of *p*-CNB with amorphous copper silicate was investigated, and each dataset was modeled using a pseudo-first-order expression:

$$\frac{d[O_3]}{dt} = -k_{obs}[O_3] \quad (1)$$

According to Fig. 7 and Table 2, *p*-CNB degradation was visibly ozone dosage dependent. The k_{obs} was increased along with the ozone dosage; particularly, the k_{obs} of 0.8 mg/L was nearly 1.5 times 0.3 mg/L, and the degradation efficiency of *p*-CNB reached the maximum (98.1%) when the ozone dosage was 0.8 mg/L. Nevertheless, the degradation efficiency of *p*-CNB decreased slightly when the ozone dosage was increased from 0.8 to 1.0 mg/L. This result suggested that 0.8 mg/L was the optimum ozone dosage for *p*-CNB degradation. The copper silicate catalyst could effectively degrade *p*-CNB with a sufficient supply of ozone, ensuring that more reactive oxygen species were generated as ozone decomposed. A further increase in ozone dosage, however, led to more O_3 and ineffective consumption of •HO, which then reacted with molecular O_3.

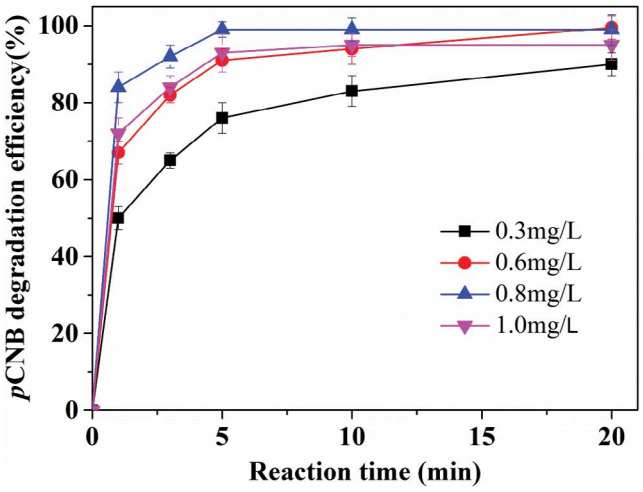

Fig. 7. Effect of ozone dosage on *p*-CNB degradation. Experiment conditions: $[p\text{-CNB}]_0$ = 100 μg/L, $[\text{catalyst}]_0$ = 100 mg/L, solution pH = 8.0, T = 20°C.

Table 2
Pseudo-first-order apparent rate constants of *p*-CNB degradation under different ozone dosages

Dosage (mg/L)	Initial pH	k_{obs} (min^{-1})	R^2
0.3	8.0	0.061	0.998
0.6	8.0	0.072	0.997
0.8	8.0	0.09	0.995
1.0	8.0	0.088	0.988

3.3.2. Effect of copper silicate dosage

In Fig. 8, the effect of copper silicate dosage on catalytic ozonation of *p*-CNB is presented. A significant increase in *p*-CNB degradation efficiency was observed from 0 to 100 mg/L catalyst dosage. The reason is that a

higher amount of the catalyst can provide more active sites during the ozonation process. However, when the copper silicate dosage was increased to more than 100 mg/L, no distinct improvement in the *p*-CNB degradation was observed.

3.3.3. Effect of humic acid dosage

Natural organic matter (NOM), which is a complex matrix of organic materials, is a key component in aquatic environments [38]. Approximately 80% of NOM is composed of high molecular weight humic acids (HAs), which may directly or indirectly react with O_3. Fig. 9 illustrates the effect of HA dosage on the degradation of *p*-CNB by copper silicate catalytic ozonation. While increasing the HA dosage from 0 to 10.8 mg/L, *p*-CNB degradation decreased from 98.1% to 90%. There was a slight decrease in the degradation efficiency of *p*-CNB caused by competition for active sites between NOM and *p*-CNB, indicating that copper silicate has great potential to be used in water purification.

3.4. Stability of amorphous copper silicate

The reusability and stability of copper silicate are important for assessing the practical application of copper silicate to the catalytic ozonation of *p*-CNB. The amorphous copper silicate was tested for stability after catalytic ozonation using catalyst powers reclaimed from the batch experiment and filtered through cellulose acetate filters of 0.45 μm. In the next experiment, the filtered catalyst was washed with ultrapure water and dried at 90°C. The decomposition results of the recovered catalysts are shown in Fig. 10a. Catalytic ozonation with amorphous copper silicate resulted in a slight drop in the degradation efficiency of *p*-CNB—specifically, from 98.1% to 90.3% after five rounds of degradation. The amorphous copper silicate showed relatively stable catalytic activity. Additionally, after catalytic ozonation by the O_3/amorphous copper silicate system, the Cu^{2+} concentrations in the filtrate were less than 0.2 mg/L after 20 min in each run, which is much lower than the limit allowed in drinking water in the United States (0.05 mg/L). To determine the stability of the

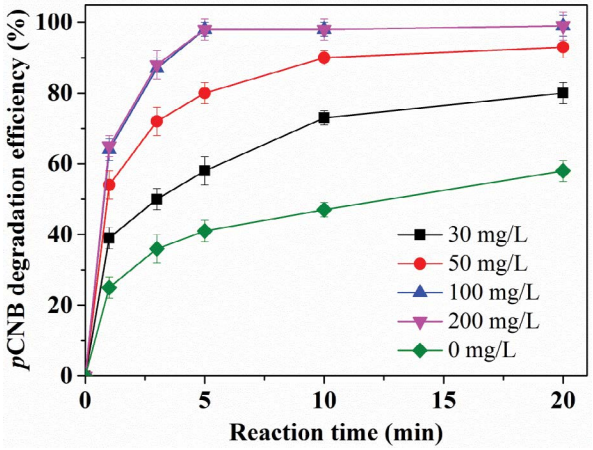

Fig. 8. Effect of catalyst dosage. Experiment conditions: $[p\text{-CNB}]_0$ = 100 μg/L, $[O_3]_0$ = 0.8 mg/L, solution pH = 8.0, T = 20°C.

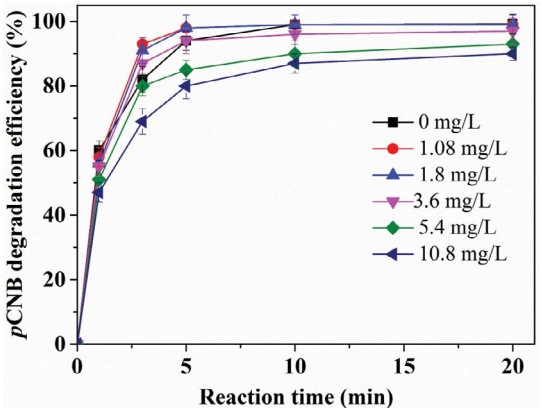

Fig. 9. Effect of humic acid dosage on *p*-CNB degradation. Experiment conditions: $[p\text{-CNB}]_0$ = 100 μg/L, $[O_3]_0$ = 0.8 mg/L, [copper silicate]$_0$ = 100 mg/L, solution pH = 8.0, T = 20°C.

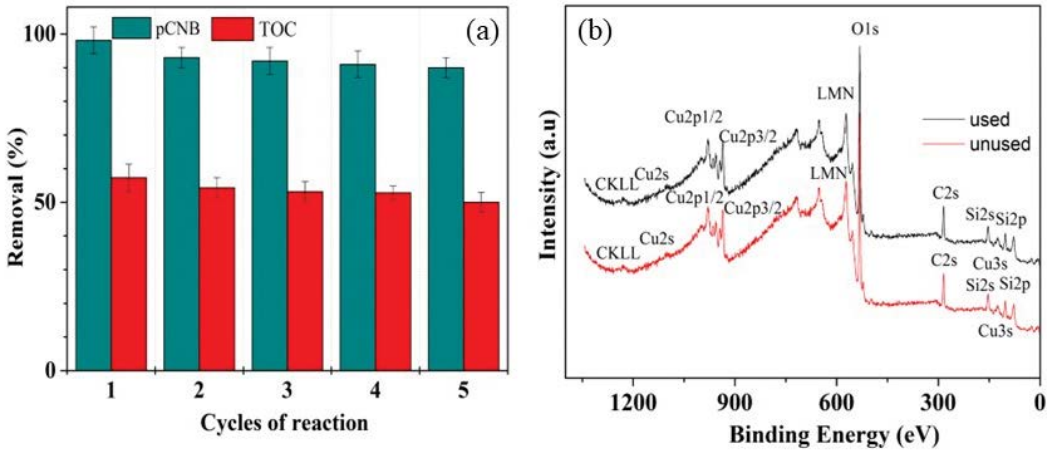

Fig. 10. (a) Effect of catalyst recycling on the ozonation of *p*-CNB. Experiment conditions were: $[p\text{-CNB}]_0$ = 100 μg/L, $[O_3]_0$ = 0.8 mg/L, [copper silicate]$_0$ = 100 mg/L, pH = 8.0 ± 0.5, reaction time = 15 min. (b) X-ray photoelectron spectroscopy patterns of used and unused copper silicate.

amorphous copper silicate used in this study, five consecutive cycles of unused and used catalysts were compared via XPS. According to Fig. 10b, the results of the used amorphous copper silicate XPS were quite similar to those of the unused copper silicate XPS sample. According to these results, copper silicate is stable in the ozonation process.

3.5. Reactive species

Since *t*-butyl alcohol (TBA) reacts rapidly with oxygen and scarcely with ozone, it is an ideal scavenger [39]. A TBA experiment was carried out to identify the contribution of •OH to the process of ozonation by copper silicate catalytic ozonation. Fig. 11 shows that with the increasing dosage of TBA, the *p*-CNB degradation efficiency decreased. As the TBA dosage was increased to 15 mg/L, the *p*-CNB removal efficiencies in both reaction systems were around 15%, indicating complete inhibition of the reaction between •OH and *p*-CNB. Based on these results, •OH is the dominant reactive species in the reaction system.

A previous study found that the surface hydroxyl groups of catalysts promote the generation of •OH [40]. According to FTIR and TG-DTG results (Fig. 5), amorphous copper silicate has abundant hydroxyl groups. The TBA experiment indicated that •OH is the predominant reactive species. Our study was designed to test the hypothesis that •OH may be generated more readily by hydroxyl groups due to their surface properties by investigating the ozonation of *p*-CNB with surface hydroxyl groups. The pH of the solution plays an important role in the decomposition of O_3 and its surface properties. Catalyst surfaces are protonated or deprotonated when the pH of the solution is below or above their point of zero charge (pH_{zpc}) [41].

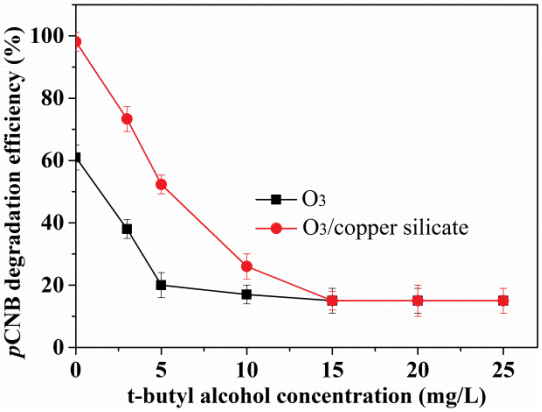

Fig. 11. Effect of *t*-butyl alcohol on the degradation of *p*-CNB. Experimental conditions: $[p\text{-CNB}]_0$ = 100 mg/L, $[O_3]_0$ = 0.8 mg/L, $[\text{copper silicate}]_0$ = 100 mg/L, pH = 8.0 ± 0.1.

Fig. 12 illustrates the results of investigating the effect of pH on the ozonation and copper silicate catalytic ozonation of *p*-CNB. The *p*-CNB degradation efficiency was strongly dependent on pH in the ozonation system. As the pH of the solution increased, the degradation efficiency increased as well. The *p*-CNB degradation was 20% at pH 3 and 61% at pH 7. In contrast, when the pH of the initial solution was 10, the *p*-CNB degradation increased to 83%. However, as shown in Fig. 12a, copper silicate catalytic ozonation curves exhibited an inflection point. In the pH range of 3 to 11, the catalyst contributed the most at pH 8.0. The pH_{zpc} of the synthesized copper silicate was 8.03. Hence, the highest degradation efficiency of copper silicate catalyzed ozonation occurred at a pH close to pH_{zpc}. Additionally, ESR analysis (inset in Fig. 12) revealed the signals of DMPO reacts with •OH (DMPO-OH) adducts with peaks in the 1:2:2:1 range, supporting the theory that •OH is the primary active species in copper silicate catalytic ozonation. In addition, when the pH was close to the pH_{zpc}, the DMPO-OH adduct signal was strongest. Based on these findings, it appeared that the higher degradation efficiency of *p*-CNB was a result of the higher concentration of •OH oxidation, due to the zero charge surface of copper silicate in the process of copper silicate catalytic ozonation.

4. Conclusions

In this study, an amorphous copper silicate catalyst was synthesized and used in a catalytic ozonation process to degrade *p*-CNB. Furthermore, to examine the morphology and physicochemical structure of amorphous copper silicate, a series of characterization techniques were applied,

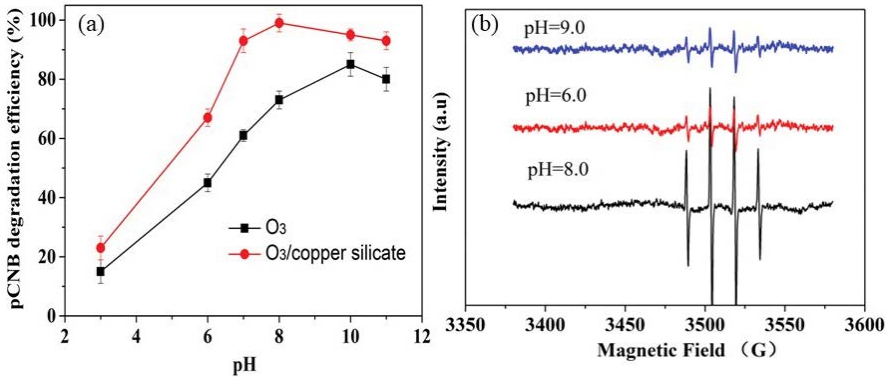

Fig. 12. (a) Effect of pH on the degradation of *p*-CNB. Experimental conditions: $[p\text{-CNB}]_0$ = 100 mg/L, $[O_3]_0$ = 0.8 mg/L, $[\text{copper silicate}]_0$ = 100 mg/L. (b) The EPR spectra of DMPO-OH from the different processes. Experimental conditions: $[\text{copper silicate}]_0$ = 500 mg/L, $[\text{DMPO}]_0$ = 100 mmol/L, $[O_3]_0$ = 2.0 mg/L.

including XRD, XPS, SEM, TEM, FTIR, TG-DTG, and BET analyses. According to the results, CuO and Cu–Si binary oxides were the main constituents of the copper silicate. After 20 min, 98.1% *p*-CNB was removed at the condition of 0.8 mg/L ozone dosage, 100 mg/L catalyst dosage, and pH 8.0. Furthermore, surface hydroxyl groups were found to be the dominant reactive radical species in radical scavenger experiments and ESR analysis. In addition, the interface reaction of O_3 with amorphous copper silicate could enhance the production of •OH, which was responsible for the enhanced ozonation. Moreover, the amorphous copper silicate was stable and could be reused five times, with a minimal amount of Cu^{2+} leaching.

Acknowledgements

This work was supported by the Natural Science Foundation of Henan [grant numbers 202300410518]; the Open Project of State Key Laboratory of Urban Water Resource and Environment [grant number QA201941]; the Zhongyuan Science and technology innovation leading talent project [grant number 224200520020]; the Nature Foundation project of Zhongyuan University of Technology [grant number K2023MS005].

References

[1] H. He, Y. Liu, D. Wu, X. Guan, Y. Zhang, Ozonation of dimethyl phthalate catalyzed by highly active Cu_xO-Fe_3O_4 nanoparticles prepared with zero-valent iron as the innovative precursor, Environ. Pollut., 227 (2017) 73–82.

[2] M. Kermani, J. Mehralipour, B. Kakavandi, Photo-assisted electroperoxone of 2,4-dichlorophenoxy acetic acid herbicide: kinetic, synergistic and optimization by response surface methodology, J. Water Process Eng., 32 (2019) 100971, doi: 10.1016/j.jwpe.2019.100971.

[3] Y. Hou, J. Ma, Z. Sun, Y. Yu, L. Zhao, Degradation of benzophenone in aqueous solution by Mn-Fe-K modified ceramic honeycomb-catalyzed ozonation, J. Environ. Sci., 18 (2006) 1065–1072.

[4] X. Huang, Y. Xu, C. Shan, X. Li, W. Zhang, B. Pan, Coupled Cu(II)-EDTA degradation and Cu(II) removal from acidic wastewater by ozonation: performance, products and pathways, Chem. Eng. J., 299 (2016) 23–29.

[5] P. Fu, L. Wang, G. Li, Z. Hou, Y. Ma, Homogenous catalytic ozonation of aniline aerofloat collector by coexisted transition metallic ions in flotation wastewaters, J. Environ. Chem. Eng., 8 (2020) 103714, doi: 10.1016/j.jece.2020.103714.

[6] G. Pavoski, F. Garjulli, C. Santos, M. Moraes, J.S. Tenório, D.C.R. Espinosa, Synthesis of a magnetic composite of silica with micro and nano-cobalt metallic structures from a spent catalyst (Co_3O_4), Mater. Sci. Eng.: B, 285 (2022) 115921, doi: 10.1016/j.mseb.2022.115921.

[7] Y. Cao, T.S. Sheriff, The oxidative degradation of Calmagite using added and in situ generated hydrogen peroxide catalysed by manganese(II) ions: efficacy evaluation, kinetics study and degradation pathways, Chemosphere, 286 (2022) 131792, doi: 10.1016/j.chemosphere.2021.131792.

[8] E. Hu, X. Wu, S. Shang, X. Tao, S. Jiang, L. Gan, Catalytic ozonation of simulated textile dyeing wastewater using mesoporous carbon aerogel supported copper oxide catalyst, J. Cleaner Prod., 112 (2016) 4710–4718.

[9] K. Luo, S.X. Zhao, Y.F. Wang, S.J. Zhao, X.H. Zhang, Synthesis of petal-like δ-MnO_2 and its catalytic ozonation performance, New J. Chem., 42 (2018) 6770–6777.

[10] M. Trapido, Y. Veressinina, R. Munter, J. Kallas, Catalytic ozonation of *m*-dinitrobenzene, Ozone Sci. Eng., 27 (2005) 359–363.

[11] Q. Dai, J. Wang, J. Yu, J. Chen, J. Chen, Catalytic ozonation for the degradation of acetylsalicylic acid in aqueous solution by magnetic CeO_2 nanometer catalyst particles, Appl. Catal., B, 144 (2014) 686–693.

[12] Z. Wu, G. Zhang, R. Zhang, F. Yang, Insights into mechanism of catalytic ozonation over practicable mesoporous Mn-CeO_x/γ-Al_2O_3 catalysts, Ind. Eng. Chem. Res., 57 (2018) 1943–1953.

[13] S. Tang, D. Yuan, Q. Zhang, Y. Liu, Z. Liu, H. Huang, Fe-Mn bi-metallic oxides loaded on granular activated carbon to enhance dye removal by catalytic ozonation, Environ. Sci. Pollut. Res., 23 (2016) 18800–18808.

[14] Z.S. Ncanana, V.R. Pullabhotla, Oxidative degradation of *m*-cresol using ozone in the presence of pure γ-Al_2O_3, SiO_2 and V_2O_5 catalysts, J. Environ. Chem. Eng., 7 (2019) 103072, doi: 10.1016/j.jece.2019.103072.

[15] L. Yuan, J. Shen, Z. Chen, Y. Liu, Pumice-catalyzed ozonation degradation of *p*-chloronitrobenzene in aqueous solution, Appl. Catal., B, 117–118 (2012) 414–419.

[16] L. Yuan, J. Shen, P. Yan, J. Zhang, Z. Chen, Catalytic ozonation of 4-chloronitrobenzene by goethite and Fe^{2+}-modified goethite with low defects: a comparative study, J. Hazard. Mater., 3655 (2019) 744–750.

[17] P.C.C. Faria, J.J.M. Órfão, M.F.R. Pereira, Activated carbon and ceria catalysts applied to the catalytic ozonation of dyes and textile effluents, Appl. Catal., B, 88 (2009) 341–350.

[18] J. Nawrocki, B. Kasprzyk-Hordern, The efficiency and mechanisms of catalytic ozonation, Appl. Catal., B, 99 (2010) 27–42.

[19] Y. Fang, Y. Guo, Copper-based non-precious metal heterogeneous catalysts for environmental remediation, Chin. J. Catal., 39 (2018) 566–582.

[20] L. Yuan, J. Shen, Z.L. Chen, X.H. Guan, Synergistic role of pumice surface composition in hydroxyl radical initiation in the catalytic ozonation process, Ozone: Sci. Eng., 38 (2016) 42–47.

[21] M.E. Mahmoud, M.F. Amira, M.E. Abouelanwar, S.M. Seleim, Catalytic reduction of nitrophenols by a novel assembled nanocatalyst based on zerovalent copper-nanopolyaniline-nanozirconium silicate, J. Mol. Liq., 299 (2020) 112192, doi: 10.1016/j.molliq.2019.112192.

[22] R.M.M. Aboelenin, N.A. Fathy, H.K. Farag, M.A. Sherief, Preparation, characterization and catalytic performance of mesoporous silicates derived from natural diatomite: comparative studies, J. Water Process Eng., 19 (2017) 112–119.

[23] P. Yan, J. Shen, L. Yuan, J. Kang, Z. Chen, Catalytic ozonation by Si-doped α-Fe_2O_3 for the removal of nitrobenzene in aqueous solution, Sep. Purif. Technol., 2281 (2019) 115766.

[24] G. Gao, J. Shen, W. Chu, Z. Chen, L. Yuan, Mechanism of enhanced diclofenac mineralization by catalytic ozonation over iron silicate-loaded pumice, Sep. Purif. Technol., 1731 (2017) 55–62.

[25] Y. Liu, Z. Chen, W. Gong, Y. Dou, W. Wang, Structural characterizations of zinc-copper silicate polymer (ZCSP) and its mechanisms of ozonation for removal of *p*-chloronitrobenzene in aqueous solution, Sep. Purif. Technol., 1721 (2017) 251–257.

[26] Z. Wang, Z. Chen, J. Chang, J. Shen, Q. Chen, Fabrication of a low-cost cementitious catalytic membrane for *p*-chloronitrobenzene degradation using a hybrid ozonation-membrane filtration system, Chem. Eng. J., 26215 (2015) 904–912.

[27] E. Laiti, L.O. OHman, J. Nordin, S. Sjöberg, Acid/base properties and phenylphosphonic acid complexation at the aged γ-Al_2O_3/water interface, J. Colloid Interface Sci., 175 (1995) 230–238.

[28] H. Bader, J. Hoigné, Determination of ozone in water by the indigo method, Water Res., 15 (1981) 449–456.

[29] B.V. Crist, Handbook of the Elements and Native Oxides, XPS International, Mountain View, CA, 1999.

[30] X. Lei, Z. Liu, J. Ding, W. Cheng, Y. Guo, X. Tang, B. Wang, Y. Huang, *In-situ* growth flower-like binder-free 3D CuO/Cu_2O-CTAB with tunable interlayer spacing for high performance lithium storage, Ceram. Int., 49 (2023) 2380–2387.

[31] M. Ye, Z. Chen, W. Wang, L. Zhen, J. Shen, Large-scale synthesis and characterization of fan-shaped rutile TiO_2 nanostructures, Mater. Lett., 62 (2008) 3404–3409.

[32] A.I. Zouboulis, P.A. Moussas, F. Vasilakou, Polyferric sulphate: preparation,characterisation and application in coagulation experiments, J. Hazard. Mater., 155 (2008) 459–468.
[33] P.T. Fanson, M.W. Stradt, J. Lauterbach, W.N. Delgass, The effect of Si/Al ratio and copper exchange level on isothermal kinetic rate oscillations for N_2O decomposition over Cu-ZSM-5: a transient FTIR study, Appl. Catal., B, 38 (2002) 331–347.
[34] M.H. Habibi, B. Karimi, Preparation of nanostructure CuO/ZnO mixed oxide by sol–gel thermal decomposition of a $CuCO_3$ and $ZnCO_3$: TG, DTG, XRD, FESEM and DRS investigations, J. Ind. Eng. Chem., 20 (2014) 925–929.
[35] F. Qi, B. Xu, Z. Chen, J. Ma, D. Sun, L. Zhang, F. Wu, Ozonation catalyzed by the raw bauxite for the degradation of 2,4,6-trichloroanisole in drinking water, J. Hazard. Mater., 168 (2009) 246–252.
[36] Y. Liu, J. Shen, Z. Chen, L. Yang, Y. Liu, Y. Han, Effects of morphous-zinc-silicate-catalyzed ozonation on the degradation of *p*-chloronitrobenzene in drinking water, Appl. Catal., A, 403 (2011) 112–118.
[37] X. Cheng, H. Liang, F. Qu, A. Ding, H. Chang, B. Liu, X. Tang, D. Wu, G. Li, Fabrication of Mn oxide incorporated ceramic membranes for membrane fouling control and enhanced catalytic ozonation of *p*-chloronitrobenzene, Chem. Eng. J., 308 (2017) 1010–1020.
[38] H. Tamura, A. Tanaka, K. Mita, R. Furuichi, Surface hydroxyl site densities on metal oxides as a measure for the ion-exchange capacity, J. Colloid Interface Sci., 209 (1999) 225–231.
[39] H. Chen, J. Wang, Catalytic ozonation of sulfamethoxazole over Fe_3O_4/Co_3O_4 composites, Chemosphere, 234 (2019) 14–24.
[40] T. Zhang, C.J. Li, J. Ma, H. Tian, Z.M. Qiang, Surface hydroxyl groups of synthetic α-FeOOH in promoting $^{\bullet}OH$ generation from aqueous ozone: property and activity relationship, Appl. Catal., B, 82 (2008) 131–137.
[41] Y. Liu, Z. Chen, X. Duan, W. Gong, G. Qin, Mechanism of heterogeneous catalytic ozonation of *p*-chloronitrobenzene in aqueous solution with iron silicate dried at different temperatures, Desal. Water Treat., 57 (2016) 19002–19009.